AIP | Review of Scientific Instruments

All fiber based multispeckle modality endoscopic system for imaging medical cavities

V. M. Murukeshan and N. Sujatha

Citation: Review of Scientific Instruments **78**, 053106 (2007); doi: 10.1063/1.2737772
View online: http://dx.doi.org/10.1063/1.2737772
View Table of Contents: http://scitation.aip.org/content/aip/journal/rsi/78/5?ver=pdfcov
Published by the AIP Publishing

All fiber based multispeckle modality endoscopic system for imaging medical cavities

V. M. Murukeshan[a] and N. Sujatha
Photonics and Microsciences Laboratory, School of Mechanical and Aerospace Engineering, Nanyang Technological University, Singapore 639798, Singapore

(Received 3 March 2007; accepted 16 April 2007; published online 31 May 2007)

Disease detection in body cavities, such as the detection of abnormal growths in the colon path, has been illustrated here using an image fiber guided catheter based multispeckle modality endoscopic system. An all fiber-optic approach for the illumination and imaging of the inner cavity walls is adopted here. An endoscope probe to carry the illumination fibers as well as the imaging lens–image fiber unit is designed and custom fabricated in order to operate the probe in its various direction sensitive configurations. This is facilitated by the selection of suitable optical elements such as beam combiner and biprism at the probe proximal end. Experimental investigations were carried out using the endoscope system employing phantom model of colon as the test specimen that has normal and abnormal (representing growth) regions and the obtained results indicated the system effectiveness in identifying the abnormal growths at an early stage. © *2007 American Institute of Physics.*
[DOI: 10.1063/1.2737772]

I. INTRODUCTION

Electronic/digital speckle pattern interferometry (ESPI/DSPI) has proven advantages in the field of nondestructive testing/imaging (NDT/I). The method is whole field, noncontact, and free from any sort of damage for the test surfaces and its applicability depends on the formation of speckles by the test surface. The applicability of speckle techniques on biosurfaces has gained much interest in the past years.[1–8] As far as the NDT/I of biosurfaces is concerned, the introduction of DSPI can offer exploring possibilities, such as detection of growths in various parts of the body. In the case of hidden body parts, such as body cavities, in order to perform DSPI, the experimental setup should be confined in an endoscope form. With the introduction of fiber optics, it is possible to design such an endoscopic DSPI system, to facilitate the abnormality/disease detection in body cavities. Such a configuration is reported in literature for identifying the elasticity difference between the soft and hard tissue parts of a porcine stomach (*in vitro*) by looking at the obtained DSPI fringe patterns.[8] The endoscope employed for that study was a standard rigid laparoscope with Hopkin's rod lens imaging scheme. There are other reported works that find applications of commercially available and rigid endoscopes in combination with DSPI.[9–11] However, in order to perform *in vivo* investigations involving hidden body cavities, a flexible-type endoscope will be more appropriate. The use of image fiber bundles instead of rigid lens systems can serve the purpose. Such endoscopes can find applications in examining medical as well as technical cavity structures. However, the resolution of image fiber has an important role in the quality of speckle fringes. A comparison on the fringe quality while using image fibers having different resolutions has been reported.[12] All the works on the endoscopic DSPI reported previously concentrate on the deformation analysis of technical/biological specimens.[11–14] However, most of the reported works employed out-of-plane configurations only. The application of in-plane DSPI in endoscopy will be helpful for the in-plane analysis of normally inaccessible (hidden) technical/medical cavity surfaces. Since shearographic configuration is considered as the most stable and reliable tool for NDT/I among all the speckle interferometric configurations, the incorporation of shear configuration in endoscopy will definitely be helpful for more accurate detection of the abnormalities.[11]

In this context, we propose a catheter endoscope system, which is capable of detecting abnormalities in all the three configurations of speckle correlation interferometry, such as in plane, out of plane, and shear. An endoscope probe that carries two illumination fibers for illumination and one "imaging lens–image fiber" unit for imaging the test cavity surface is designed here, in order to incorporate the illumination and imaging geometries necessary for all the configurations. The efficiency of the probe in detecting abnormalities in all the three configurations has been illustrated and compared with each other, employing a phantom model of colon as the test cavity surface.

II. ENDOSCOPE SYSTEM FOR SPECKLE CORRELATION INTERFEROMETRY: DESIGN CONSIDERATIONS

The endoscope system consisted of four main sections/elements: (i) the endoscope probe, (ii) the collection lens, (iii) the optical element to facilitate the individual interferometric configurations, and (iv) charge coupled device (CCD) camera and the associated image processing system. Schematic diagram of the endoscope system is shown in Fig. 1.

[a]Author to whom correspondence should be addressed; electronic mail: mmurukeshan@ntu.edu.sg

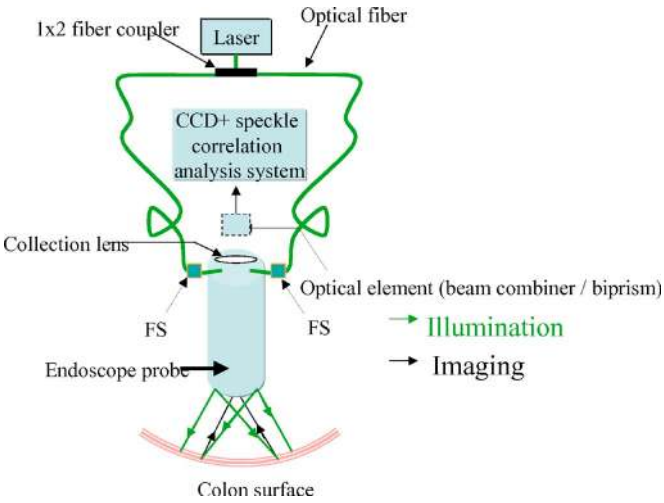

FIG. 1. Schematic of the endoscope system. FS—finger splice (connector).

Light from the 30 mW laser source (532 nm) is coupled into a sheathed single mode fiber, which is then split into two sheathed single mode fibers via a 1×2 fiber coupler/splitter. The laser employed here is a diode pumped solid state (DPSS) cw laser. The two sheathed fibers are connected to two bare single mode (SM) fibers (with 1 mm removable sheath) via connectors known as finger splices (FSs). These bare fibers with protective thin sleeves are then fed into the illumination channels of the probe. Also, these fibers are well supported (shown in Fig. 2) by specially designed components inside the distal end. This type of arrangement allows the easy plug-in and plug-out of the probe and the source. The source light is delivered to the colon surface from the fiber ports at the probe distal end. It is to be noted that the laser power at the end of the fiber outputs are in the range of 7–10 mW. The two illumination fibers are oriented at equal angles to the axis of the imaging fiber, so as to make the center of the illuminated/excited area in line with the imaging unit. A closer view of the probe distal end and its different parts such as image lens port and channels for illumination along with their respective dimensions is given in Fig. 2. The illumination fibers and image fiber are supported in their respective channels, as shown in Fig. 2. The return light from the colon surface is collected by an imaging lens and is transmitted through an image fiber (Fujikura 15-600N, 600 μm diameter, 15 000 pixels, lateral resolution=25 pixels/μm). A ball lens is used in the endoscope as the imaging lens due to its excellent symmetry along the probe axis. The diameter of the ball lens is chosen to be 3 mm in order to minimize the barrel distortion due to small diameter lenses, as illustrated in Fig. 3. Figure 3(a) represents the standard USAF resolution chart imaged using the image fiber–3 mm diameter ball lens combination and Fig. 3(b) represents the same when the 3 mm ball lens was replaced with a lens of 0.7 mm diameter. The targeted diameter was 5×5 mm^2 with the probe to target distance of 20 mm. It is also to be mentioned that there is no additional aperture control at this and hence on the speckle size. The chosen lens diameter also helps us to keep the overall probe diameter at 10 mm, excluding the outer cover. An objective lens (Mitutoyo infinity corrected 20× objective with 20 mm working distance) placed at the proximal end of the probe collects the return image/light from the image fiber and directs them to the CCD attached to the image processing system (EDC-2000N computer camera system). Depending on the interferometric configuration (in plane, out of plane, or shear) suitable optical element such as a beam combiner or biprism is inserted between the collection lens and the CCD.

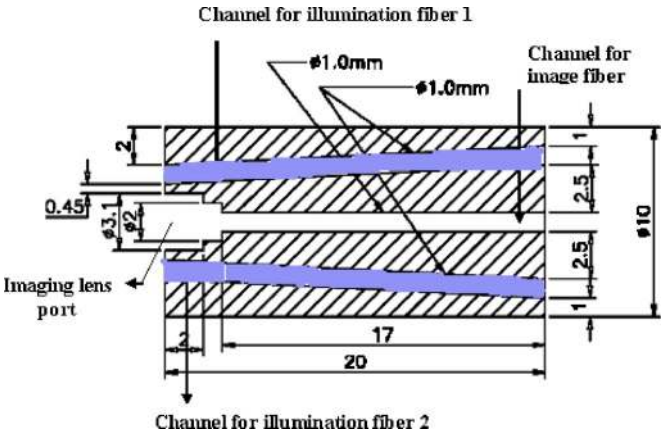

FIG. 2. Dimensions of the endoscope probe distal end.

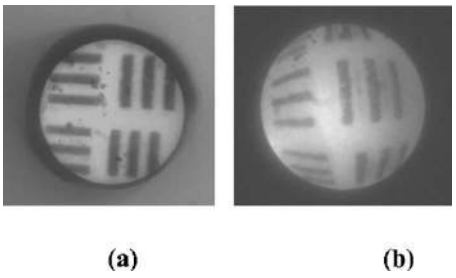

FIG. 3. USAF resolution chart imaged using the proposed system: (a) ball lens of 3 mm diameter and (b) lens with 0.7 mm diameter.

III. THEORY OF SPECKLE FRINGE FORMATION

The fringe formation in ESPI/DSPI is based on the intensity correlation of the speckle patterns before and after object deformation. Let I_1 and I_2 be the intensities of the two beams interfering with each other. Then the total intensity of the two beams, before applying object deformation, is given by[2]

$$I = I_1 + I_2 + 2(I_1 I_2)^{1/2} \cos\phi, \tag{1}$$

where ϕ is the phase difference between the two beams.

The total intensity after deformation is given by[2]

$$I' = I_1 + I_2 + 2(I_1 I_2)^{1/2} \cos(\phi + \Delta\phi), \tag{2}$$

where $\Delta\phi$ is the additional phase change introduced due to the specimen deformation.

Though the calculation of $\Delta\phi$ in the case of flat surfaces is well reported in literature,[2,3] it is not the same case as far as curved surfaces are concerned. An extended theory was proposed recently by our group to explain the speckle fringe formation in curved surfaces.[15]

By applying subtractive speckle correlation, the total intensity is given by[2]

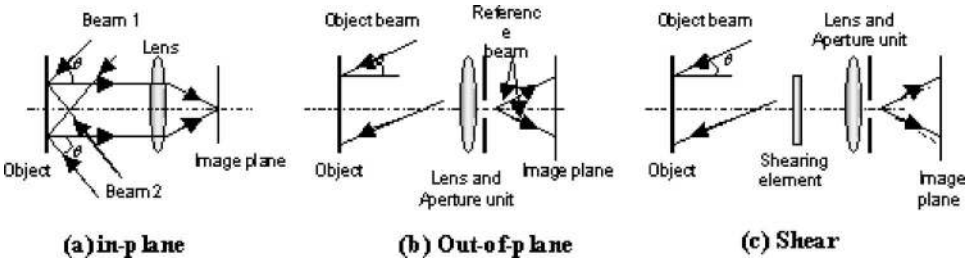

FIG. 4. Schematic diagram showing the illumination directions, illumination angle, and viewing directions for three configurations: (a) in-plane, (b) out-of-plane, and (c) shear configurations.

$$\text{total intensity} = 4(I_1 I_2)^{1/2} |\sin(\phi + \Delta\phi/2)\sin(\Delta\phi/2)|. \quad (3)$$

Dark fringes are formed when

$$\Delta\phi = 2m\pi \quad (4)$$

and bright fringes are formed when

$$\Delta\phi = (2m+1)\pi. \quad (5)$$

The phase change at the image plane due to the object deformation can be calculated with respect to the initial undeformed point of the specimen surface, which is subjected to maximum deflection upon loading.

The total deformation of the specimen on random loading will have all the three deformation components and is given by

$$\mathbf{L} = u\mathbf{i} + v\mathbf{j} - w\mathbf{k}, \quad (6)$$

Where u, v, and w represent the deformation of the specimen along X, Y, and Z directions, respectively, upon the application of an external perturbation and **i**, **j**, and **k** are the unit vectors along X, Y, and Z directions. The illumination directions, illumination angle, and viewing directions for three configurations are shown in Fig. 4.[2,3] This is the case for a flat surface specimen. However, medical cavities such as inside colon are a typical curved surface specimen. So in our analysis we have to consider the deformation components of a curved surface with the deformation vector to be derived in cylindrical coordinates. Depending on the type of loading, the displacement **L** of any point in the specimen can be resolved along r (radial), θ (tangential), and a (axial) directions and are denoted as w_r, w_θ, and w_a. The unit vectors in cylindrical coordinates are denoted as $\mathbf{e}_r$, $\mathbf{e}_\theta$, and $\mathbf{e}_a$, as shown in Fig. 5. Therefore, the deformation vector of the specimen point P upon random loading is given by

$$\mathbf{L} = w_\theta \mathbf{e}_\theta + w_a \mathbf{e}_a - w_r \mathbf{e}_r. \quad (7)$$

Now, let the total deformation of a point P be represented by W_T, which is the vector sum of the three deformation components, i.e.,

$$W_T = [(w_\theta)^2 + (w_r)^2 + (w_a)^2]^{1/2}. \quad (8)$$

The axial component w_a does not contain any curvature information and can be considered as similar to the Y-direction displacement component of the flat specimen (v). These details on the extended theoretical formulations along with the radial and tangential deformation components containing the specimen curvature information in the three significant speckle interferometric configurations are reported by us elsewhere already.[15]

Through this article we intend to illustrate the design, fabrication, and experimental verification of an all fiber-optic catheter endoscopic system for imaging curved inner surfaces of the medical cavities, such as colon.

IV. EXPERIMENTAL METHODS

In order to illustrate the probe efficiency in detecting the abnormalities present in the body cavities, experimental investigation using the developed endoscope system (described in Sec. II) is carried out on the normal and abnormal (with simulated growth) phantom colon model, the preparation of which is discussed below.

A. Preparation of the phantom colon tissue model

The phantom colon model (purchased from Buy-A-Mag Corporation),[16] which resembles the realistic human colon, is used as the test specimen. At different locations inside this phantom colon, tailor made layers of phantom tissues are pasted, which were obtained from Simulab Corporation.[17] The tissue layers are having a thickness, each equal to the layer thickness of the real colon (approximately 1 mm).[18] The significance of the proposed concept is on the laser biospeckles, such as laser speckles formed due to random interference of waves emanating from the tissue/biological surface, produced at the colon inner walls. Hence what is more important is the coherent light (such as laser) illumination and hence the correct incident laser wavelength for bio-

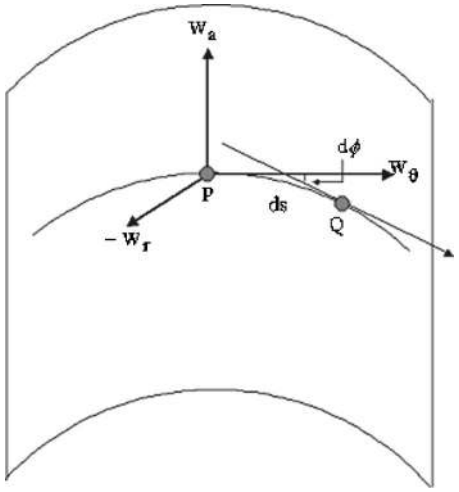

FIG. 5. Different displacement components for a cylindrical specimen (ds: elemental displacement along the curved surface, $d\phi$: angle between the tangents at points P and Q, w_r: displacement component along radial direction, w_θ: displacement component along tangential direction, and w_a: displacement component along axial direction).

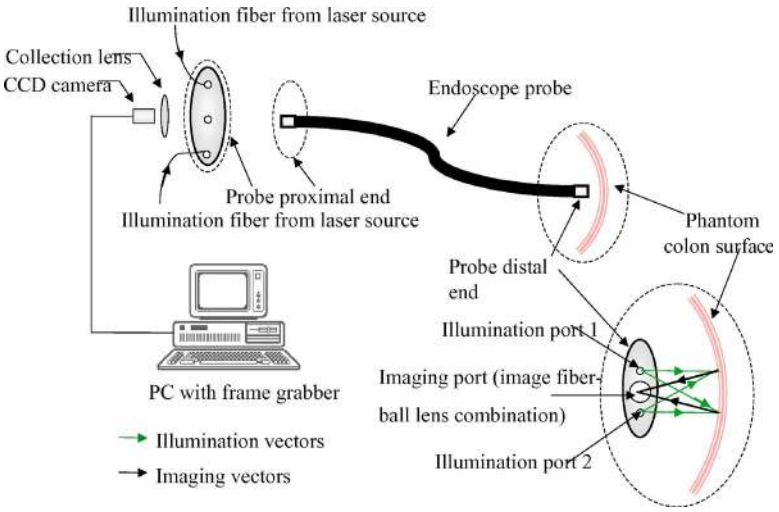

FIG. 6. Schematic diagram of the endoscope system—in-plane configuration.

speckle formation as well as detector that has good sensitivity to the said wavelength. At this chosen wavelength of 532 nm, the speckle patterns formed are of high contrast and can also be attributed to the sensitivity of the CCD camera to this wavelength. Also, we have used the laser power density of ≈ 10 mW/cm^2 in such a way that it meets well within the standard of laser tissue interaction in terms of threshold power density (i.e., 25 mW/cm^2 at the maximum).

In order to simulate abnormality/growth, the phantom tissue material of 1 mm thickness representing the abnormality is introduced between the first and second tissue layers. A total of four tissue layers are taken representing the real colon layers. The size of the tissue material to represent the abnormality is chosen to be either 1 mm (to represent small abnormality) or 3 mm (to represent larger abnormality). After introducing the abnormality, the layers are pasted together, and introduced into the phantom model.

B. The endoscope system in the in-plane configuration

The schematic diagram of the endoscope system in the in-plane configuration along with the illumination directions of the two illumination ports of the endoscope probe is shown in Fig. 6 and the corresponding laboratory prototype is shown in Fig. 7. In this configuration the two fiber-optic arms of the laser source are connected to the illumination fiber ports of the endoscope probe using finger splices, as discussed in Sec. II. The reflected speckle pattern is collected by the ball lens and transmitted through the image fiber. The collection lens placed after the probe proximal end collects the speckle pattern transmitted through the image fiber. This collected speckle pattern is allowed to fall on a CCD placed behind the collection lens. The image/speckle pattern is digitized by the CCD and fed to the computer installed with the frame grabber.

C. The endoscope system in the out-of-plane configuration

The schematic diagram of the endoscope system in the out-of-plane configuration is shown in Fig. 8 and the corresponding laboratory prototype is shown in Fig. 9. In this configuration, only one of the fiber ports is used for illuminating the curved colon phantom surface. The reflected speckle pattern is collected by the ball lens and transmitted through the image fiber. The collection lens after the probe proximal end collects the speckle pattern transmitted through the image fiber. This collected speckle pattern is combined with the reference beam (supplied by the other illumination fiber from the laser) at the beam combiner, placed between the collection lens and the CCD camera. The reference beam is attenuated before it reaches the beam combiner using an attenuator (variable neutral density filter). The CCD placed behind the beam combiner then captures the reference beam combined with the reflected image.

D. The endoscope system in the shear configuration

The schematic diagram of the endoscope system in the shear configuration is shown in Fig. 10 and the corresponding laboratory prototype is shown in Fig. 11. In this configuration, one of the fiber ports is used for illuminating the curved phantom surface. The reflected speckle pattern is collected by the ball lens and transmitted through the image fiber. The collection lens after the probe proximal end collects the speckle pattern transmitted through the image fiber. This collected speckle pattern is sheared into two by means of a biprism (1° wedge angle) inserted between the collection

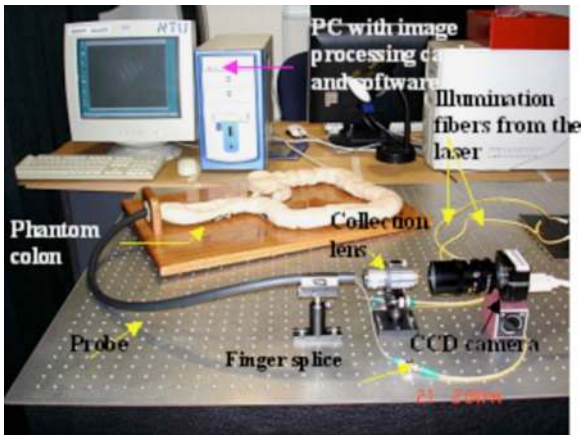

FIG. 7. Developed probe: laboratory prototype—in-plane configuration.

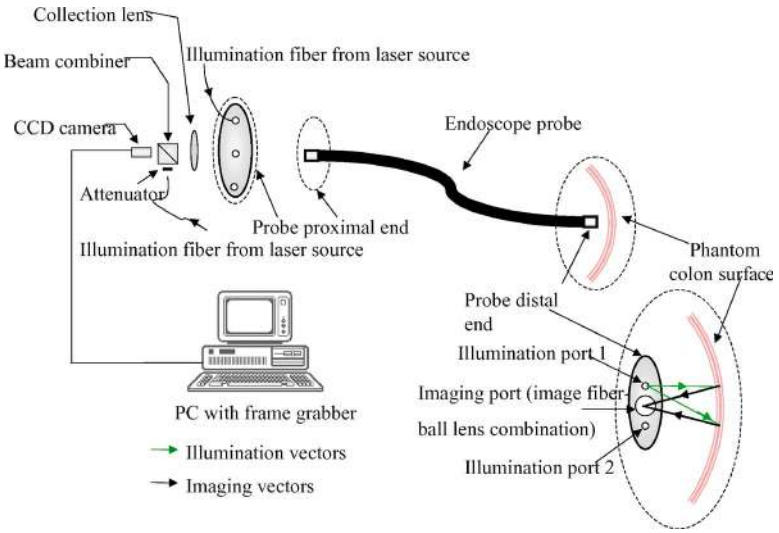

FIG. 8. Schematic diagram of the endoscope system—out-of-plane configuration.

lens and the CCD. The sheared speckle patterns are allowed to fall on a CCD placed directly behind the biprism.

For all the above explained speckle interferometric configurations, the speckle pattern captured by the CCD is stored in a frame buffer and displayed in the personal computer (PC) monitor in real time with the help of a developed software. Frame corresponding to the initial state of the phantom colon model is stored as the reference frame and subsequent frames corresponding to the different states of the object are subtracted from the first frame at the rate of 25 frames/s. The evolution of fringes is observed on a PC monitor in real time, using the developed software and EDC 2000N image-processing card. Very minute load is sufficient for generating speckle fringes. It is to be mentioned that the option of pneumatic load is chosen here for giving perturbation as used for opening the rectal walls.

V. RESULTS AND DISCUSSIONS

Experiments were carried out with the endoscope system in the in-plane, out-of-plane, as well as shear configurations to illustrate the ability of the system for the detection of abnormalities present in the biological cavities, employing the normal and abnormal phantom colon models. It is to be mentioned that though the targeted imaged area was 5 $\times 5$ cm^2, the fringes formed at the respective simulated abnormality sites were the target of this study.

Figure 12(a) represents the in-plane fringe pattern for a normal colon phantom, where the fringes followed straight-line nature. Figure 12(b) shows the in-plane fringe patterns obtained for the abnormality colon phantom (simulated growth size of 3 mm). Here the position of abnormality is indicated by the presence of a kink in the fringe pattern. It is noted that when the endoscope system was set in the in-plane configuration, abnormality size less than 3 mm was difficult to be identified. Smaller abnormalities required more number of in-plane fringes, with which the significant identification of the kink can be made.

Figure 13(a) represents the fringe pattern for a normal colon phantom, when the endoscope system was set in the out-of-plane configuration. Here the fringes followed the pattern of concentric ovals. Figure 13(b) shows the fringe patterns obtained for the colon phantom with simulated growth (size of 3 mm), using the endoscope system in the out-of-plane configuration. Here the position of abnormality is indicated by the presence of a kink in the fringe pattern. Similar to the in-plane setup, it is noted that when the endoscope system was set in the out-of-plane configuration, growth size of less than 3 mm was difficult to be identified. Smaller abnormalities required more number of out-of-plane fringes to be formed to identify the kink, representing the growth location. But this poses hindrance for both in-plane and out-of-plane configurations, as optimization of external perturbation and other speckle imaging parameters resulted in the decorrelation of speckle patterns.

As reported recently, fringe pattern of the shape of a butterfly was expected to be formed from the phantom model (from its curved inner surface) when the endoscope system was set up in the shear configuration.[15,19] Figure 14(a) shows such a fully developed butterfly fringe pattern from the curved inner surface of the phantom colon that was imaged using a conventional stereographic setup. Only a small area is imaged when the endoscope was set in the shear configuration, which is the central region of the butterfly fringe pat-

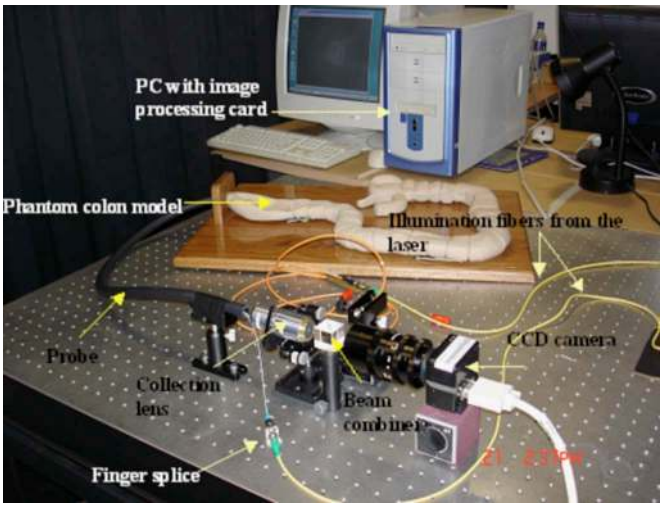

FIG. 9. Developed probe: laboratory prototype—out-of-plane configuration.

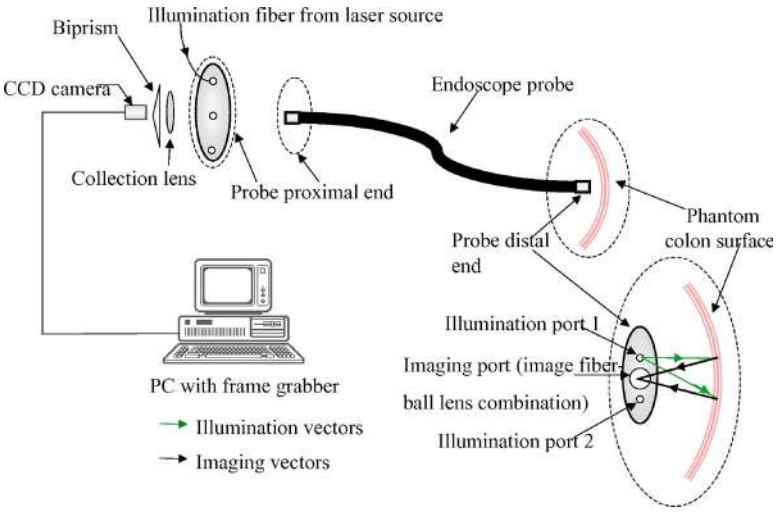

FIG. 10. Schematic diagram of the endoscope system—shear configuration.

tern, as shown in Fig. 14(b). Figures 14(c) and 14(d) show the shear fringe pattern obtained for the abnormal colon phantom having growth size of 1 mm, using the endoscope. Here also, the imaged area falls under the central region of the fully developed butterfly fringe pattern. In Fig. 14(c) the position of abnormality is seen as a kink in the fringe pattern, whereas Fig. 14(d) represents a separate fringe system formed at the position of the abnormality upon increased external perturbation/deformation of the phantom specimen.

In the shear configuration, the presence of abnormality created a separate fringe system upon the decorrelation of the original fringe system, as the specimen deformation is increased, irrespective of the defect size. In this way, identification of smaller abnormalities (≈1 mm) was possible with the endoscope system in the shear configuration. It is to be noted that more specimen deformation resulted in the decorrelation of fringe patterns for both out-of-plane as well as in-plane configurations. Since the abnormality was represented as a kink in the original fringe system, decorrelation of the same made the abnormality identification impossible in these configurations. Regarding the thickness of abnormalities, abnormalities of very small thickness such as 1 mm were detectable by all the endoscopic DSPI configurations. However, growth sizes less than 3 mm were unable to be detected by using both the in-plane and out-of-plane configurations. A comparison of in-plane, out-of-plane, and shear configurations based on their abnormality detection capability is given in Table I.

The abnormality detection efficiency depends on the fringe quality also. As far as the quality of the obtained fringe patterns is concerned, it very much depends on the employed configuration, spatial resolution of the camera, and speckle size. The abnormalities were not clearly visible in the results obtained with Fig. 6 or Fig. 7 configuration while it is very evident with Fig 8. The abnormality obtained as kink in Fig. 13 is very evident whereas it is a bit obscure in Fig. 12 as expected. We have highlighted the region in circle in the print. In real-time experiment one need not have that circle to identify those regions, as the monitor resolution is much higher than the print resolution. It is to be mentioned that the formation of kink can be attributed to the variation in the localized elasticity due to the presence of abnormalities. It is proven that the abnormality detection with the derivative configuration (Fig. 10 or Fig. 11) is better when compared to

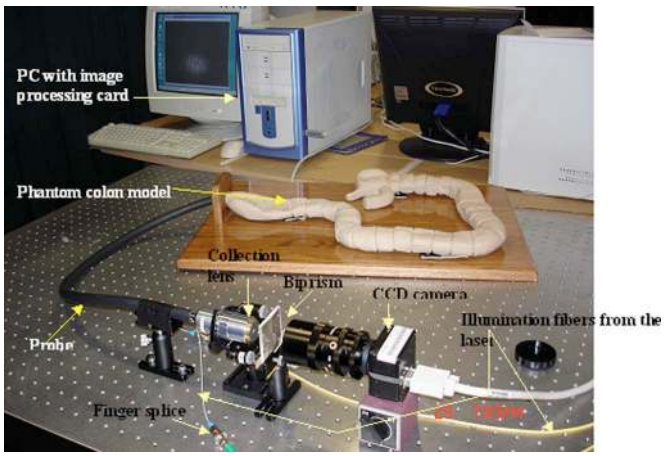

FIG. 11. Developed probe: laboratory prototype—shear configuration.

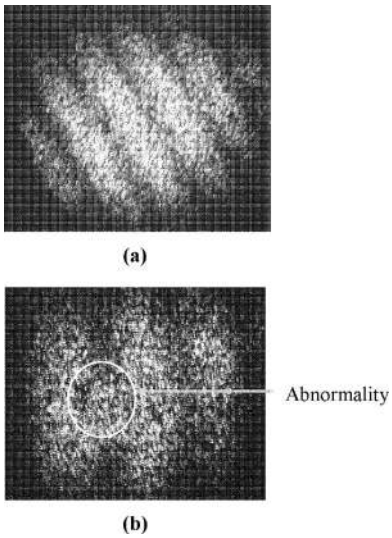

FIG. 12. In-plane fringes obtained using the endoscope system: (a) fringes obtained from normal colon phantom model and (b) fringes obtained from abnormal colon phantom model.

TABLE I. Comparison of the three different endoscopic DSPI configurations for abnormality detection efficiency.

DSPI configurations	In plane	Out of plane	Shear
Representation of abnormality	Kink in the fringe system	Kink in the fringe system	Kink in the fringe system/separate fringe system at the abnormality site
Surface/subsurface growth (abnormality) (size ⩾3 mm; thickness 1 mm)	Detectable	Detectable	Detectable
Surface/subsurface growth (abnormality) (size <3 mm; thickness 1 mm)	Not detectable	Not detectable	detectable

the direct displacement configurations (Fig. 6 or Fig. 7 and Fig. 8 or Fig. 9) with illustration of step by step fringe formation (Fig. 14) at the abnormality site.

VI. CONCLUSIONS

An endoscope system capable of identifying the presence of abnormalities in the cavities of difficult access, such as colon, using speckle interferometric techniques has been developed and experimentally illustrated. The design of the endoscope was based on an all fiber-optic approach, thus making the probe flexible enough to enable examination of the hidden body parts. The illumination and imaging ports in the endoscope were arranged in a special way so as to set up the whole endoscope system in the in-plane, out-of-plane, as well as shear configurations. Very minute load is sufficient for generating speckle fringes. It is to be mentioned that the option of pneumatic load is chosen here for giving perturbation as later the same pneumatic channel (as in a generic endoscope), which is used for opening the rectal walls, will be used for perturbation.

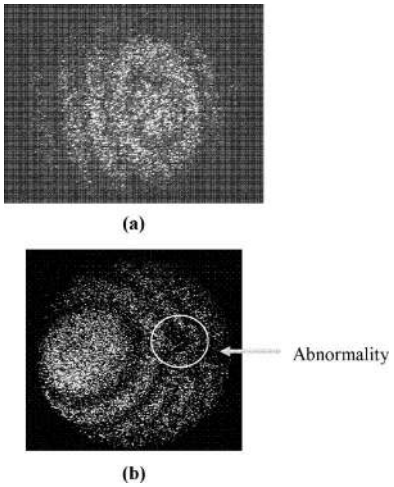

FIG. 13. Out-of-plane fringes obtained using the endoscope system: (a) fringes obtained from normal colon phantom model and (b) fringes obtained from abnormal colon phantom model.

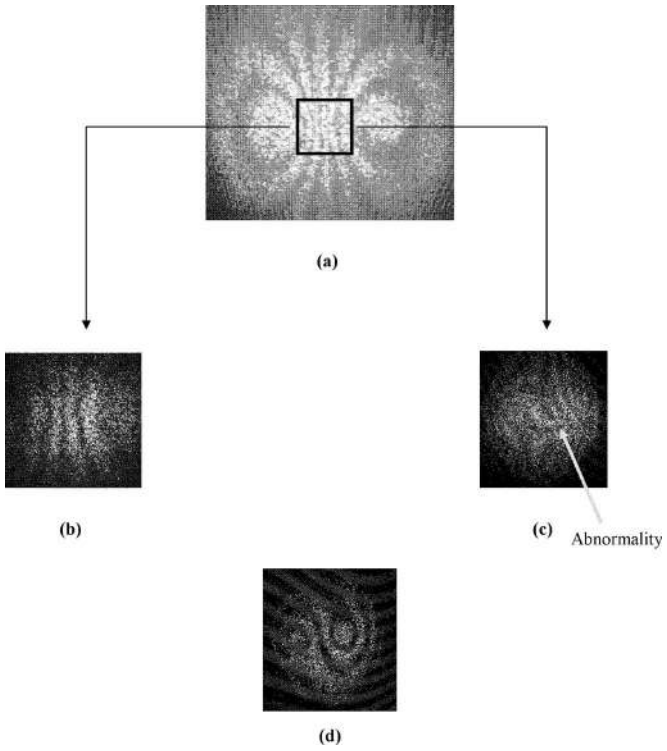

FIG. 14. (a) Fully developed shear fringe obtained from a curved tissue using conventional shear configuration; (b) shear fringes obtained using the endoscope system from normal colon phantom model; (c) shear fringes obtained using the endoscope system from abnormal colon phantom model with a kink at the abnormality site; (d) separate shear fringe system evolved at the abnormality site, captured using the endoscope.

Thus we have demonstrated abnormal growth detection efficiency with a novel endoscope capable of operating in three different speckle correlation modalities, which can be applied for the inspection of intracavities such as colon. This proposed probe system is flexible and uses a specially designed and custom made image fiber–lens unit along with illumination fibers configured as shown in Fig. 2, so as to meet the operation in the illustrated three speckle imaging modalities. The abnormality detection capabilities of each of the configurations were compared with each other, using the endoscope system in a phantom model of colon with simulated abnormalities. It is illustrated that the detection efficiency is higher and more significant in the shear configuration when compared to the in-plane and out-of-plane sensitive configurations. The abnormalities (growth) simulated in the phantom colon model resembled the early stages of cancer growth, thus making the endoscope system effective in identifying the presence of cancer at an early stage.

Due to semitransparent properties of tissues the reflection from the underneath layers may cause a reduction in speckle contrast as well as the contrast of the subtraction fringes. Also, the effect of image fiber in the total contrast is an issue to be considered. Furthermore, the effect of blood flow in tissues and vapor contents inside the colon also needs to be analyzed. These above mentioned aspects of the problem will be studied in detail in the next phase of this research

work. Quantitative phase evaluation methodologies such as phase shifting approaches will also be looked into in the future.[9,11,12] This may open up additional possibilities of automated data analysis that can make this system a more user friendly chair side unit for the medical practitioners.

It is to be mentioned that these approaches can also find applications in technical cavities such as inspection of pressure vessels.

ACKNOWLEDGMENT

The authors acknowledge the financial support received through Academic Research Fund (RG10/02, 18/05), Nanyang Technological University, Singapore.

[1] Y. Aizu and T. Asakura, Opt. Laser Technol. **23**, 205 (1991).
[2] T. Kreis, *Holographic Interferometry: Principles and Methods* (Akademie-Verlag, Berlin, 1996).
[3] A. Vogel, Optik (Jena) **72**, 95 (1986).
[4] W. Steinchen and L. Yang, *Digital Sheorgraphy: Theory and Applications of Digital Speckle Pattern Shearing Interferometry* (SPIE, Bellingham, 2003).
[5] O. J. Lokberg, K. Hogmoen, and O. M. Holige, Appl. Opt. **18**, 763 (1979).
[6] A. Kishen, V. M. Murukeshan, V. Krishnakumar, C. S. Lim, and A. Asundi, Opt. Lasers Eng. **39**, 489 (2003).
[7] J. F. Roman, V. Moreno, and J. R. Salgueiro, Proc. SPIE **2628**, 184 (1995).
[8] B. Kemper, D. Dirksen, W. Avenhaus, A. Merker, and G. V. Bally, Appl. Opt. **39**, 3899 (2000).
[9] W. Avenhaus, B. Kemper, S. Knoche, D. Domagk, C. Poremba, G. von Bally, and W. Domschke, Lasers Med. Sci. **19**, 223 (2005).
[10] S. Knoche, B. Kemper, P. Langehanenberg, M. Noll, K. Irion, and G. von Bally, DGaO Proceedings, 2005 (unpublished); http://www.dgaoproceedings.de.
[11] M. Schuth, F. Vössing, and L. Yang, Journal of Holography and Speckle **1**, 46 (2004).
[12] S. Schedin, G. Pedrini, H. J. Tiziani, and A. K. Aggarwal, Appl. Opt. **40**, 2692 (2001).
[13] M. Facchini, P. Zanetta, D. Paoletti, and G. Schirripa Spagnolo, Optik (Jena) **95**, 27 (1993).
[14] S. Schedin, G. Pedrini, H. J. Tiziani, and F. M. Santoyo, Opt. Commun. **165**, 183 (1999).
[15] M. V. Matham and N. Sujatha, Appl. Opt. **43**, 2400 (2004).
[16] Homepage of Buy-a-mag corporation, www.buyamag.com
[17] Homepage of Simulab corporation, www.simulab.com
[18] C. H. Huh, M. S. Bhutani, E. B. Farfan, and W. E. Bolch, Physiol. Meas **24**, 15 (2003).
[19] N. Sujatha and V. M. Murukeshan, Opt. Eng. (Bellingham) **43**, 3055 (2004).